Acta Universitaria
ISSN: 0188-6266
actauniversitaria@ugto.mx
Universidad de Guanajuato
México

Ramírez-Manzanares, Alonso; Patiño, Jonathan Rafael; Ashtari, Manzar
Denoising of brain DW-MR data by single and multiple diffusion kernels
Acta Universitaria, vol. 20, núm. 3, septiembre-diciembre, 2010, pp. 44-50
Universidad de Guanajuato
Guanajuato, México

Acta Universitaria
DIRECCIÓN DE APOYO A LA INVESTIGACIÓN Y AL POSGRADO
CIENCIAS DE LA SALUD

Universidad de Guanajuato

Denoising of brain DW-MR data by single and multiple diffusion kernels

Alonso Ramírez-Manzanares, Jonathan Rafael-Patiño*, Manzar Ashtari***

ABSTRACT

Diffusion Weighted Magnetic Resonance Imaging is widely used to study the structure of the fiber pathways of white matter in the brain. However, the recovered axon orientations can be prone to error because of the low signal to noise ratio. Spatial regularization can reduce the error, but it must be done carefully so that real spatial information is not removed and false orientations are not introduced. In this paper we investigate the advantages of applying an anisotropic filter based on single and multiple axon bundle orientation kernels. To this end, we compute local diffusion kernels based on Diffusion Tensor and multi Diffusion Tensor models. We show the benefits of our approach to three different types of DW-MRI data: synthetic, in vivo human, and acquired from a diffusion phantom.

RESUMEN

Las imágenes por resonancia magnética pesadas en difusión son ampliamente utilizadas para el estudio de las estructuras cerebrales dentro de la materia blanca del cerebro. Sin embargo, recuperar las orientaciones de los axones puede ser susceptible a errores por el ruido dentro de la señal. Una regularización espacial puede mejorar la estimación, pero debe ser realizada cuidadosamente dado que puede remover información espacial ó introducir falsas orientaciones. En este trabajo se investigaron las ventajas de aplicar un filtro anisotrópico basado en simples y múltiples kerneles de orientación de manojos de axones. Para esto, hemos calculado kerneles locales de difusión basados en modelos de tensores de difusión y multi tensores de difusión. Mostraremos los beneficios de nuestra propuesta en 3 tipos diferentes de imágenes obtenidas por resonancia magnética pesada en difusión: Datos sintéticos, imágenes humanas tomadas en vivo, y datos obtenidos de un fantasma simulador de difusión.

Recibido: 28 de Julio de 2010
Aceptado: 18 de Octubre de 2010

INTRODUCTION

One of the most challenging goals in neuroimaging is the estimation of connectivity patterns in the brain in vivo. For this purpose, a special magnetic resonance imaging (MRI) technique named Diffusion Weighted Magnetic Resonance Imaging (DW-MRI) is used. In this technique, it is possible to obtain an estimation of the orientation of water diffusion in a tissue specimen. Specifically in the brain, such diffusion is constrained by the direction of nerve bundles. This information is very useful in neuroscience research due to the relationship of brain connectivity with several diseases and, in general, with brain development (Poldrack 2007).

The DW–MRI acquisition protocol measures (indirectly) the Probability Density Function (PDF) or Ensemble-Average Probability (EAP) $P(\mathbf{x})$ for the displacement vector $\mathbf{x}=\mathbf{x}_e-\mathbf{x}_0$ corresponding to the particle displacement located at $\mathbf{x}_0$ at the beginning and at $\mathbf{x}_e$ at the end of the experiment for a fixed time τ.

Palabras clave:
Resonancia magnética pesada en difusión, MRI, Filtrado de ruido, Tensor de difusión, Multi-tensor, Filtrado anisotrópico, DWI.
Keywords:
Diffusion, Weighted, MRI , Denoising, Diffusion tensors, Multi-tensor, Anisotropic filtering, DWI.

The Fourier transform relationship between the PDF and the DW–MR signal for a voxel is given by (Alexander, 2005):

$$S(q_k,\tau) = S_0 \int_{R^3} P(x)\exp(-i\tau q_k^T x)dx + \varepsilon_k \quad (1)$$

* Departamento de Matemáticas, División de Ciencias Naturales y Exactas, Campus Guanajuato, Universidad de Guanajuato. Callejón Jalisco S/N Guanajuato, Gto. Correos electrónicos: alram@cimat.mx. jonhrafe@cimat.mx.
** Diffusion Tensor Imaging and Brain Morphometry, Lab. Children's Hospital of Philadelphia. 3535 Market St. 14th Floor, Room 1418, Philadelphia PA, 19104. E-mail: ashtari@email.chop.edu.

Where S_0 is the measured signal when no diffusion magnetic field gradient is applied, $S(\boldsymbol{q}_k,\tau)$ is the observed attenuated signal value given the Diffusion Encoding Orientation (DEO) vector $\boldsymbol{q}_k=\gamma\delta G\mathbf{g}_k$ where γ is the gyromagnetic ratio, δ is the applied time for the directional magnetic gradient, G is the magnitude of the applied diffusion magnetic field gradient and the unitary 3D vector $\mathbf{g}_k$ indicates the k=1,…,M orientation of the diffusion–encoding gradients. $\mathcal{E}_k$ is the signal noise. R^3 denotes the three dimensional real space. Finally τ is the effective diffusion time. A standard acquisition protocol for a single orientation $\mathbf{g}_k$, gives a 3D image, where in each voxel, the intensity indicates the grade of attenuation in the signal. Lower gray values indicate larger attenuations (S is smaller) and this indicates significant water diffusion in the configured orientation (Figure 1).

Given that the image pixels are the magnitude of the associated complex MR signal with additive Gaussian noise in both real and imaginary components, the signal noise ε_k in (1) has Rician distribution (Gudbjartsson, 1995). We show three examples of *in vivo* DW-Signals (Figure 2) for M=64 Diffusion Encoding Orientation measurements.

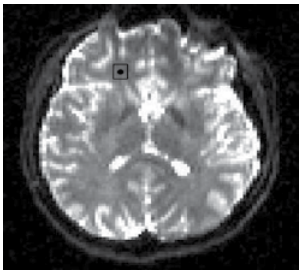

Figure 1. An axial slice from a DW brain scan for a 3D orientation gk, red spot indicates the position x =55, y = 87, z =36 where the signals of figure 2 where taken. The dark zones correspond to brain sites where the water diffusion is significant along gk.

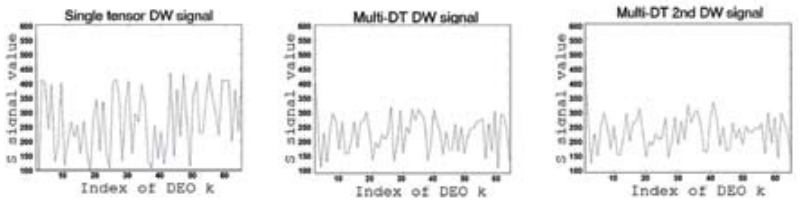

Figure 2. Three DW signals from different image positions composed of S0 and M =64 S(qk , τ), k = 1, 2, . . . , M DEO. The middle and right signals correspond to neighboring voxels.

The axon bundle orientation estimation problem can be stated as the estimation of $P(\mathbf{x})$ based on as few as possible measurements $S(\mathbf{q}_k,\tau)$. The Ensemble-Average Probability $P(\mathbf{x})$ can be estimated in a parametric fashion, by assuming some observation model, or can be estimated in a non-parametric way (Alexander, 2005). In any case, the noise present in the DW signal perturbs the axon fiber orientation estimation, as well as the estimations of anisotropy measurements of diffusion per voxel. For this reason, in the recent past, there has been a flurry of activity on denoising the diffusion information in terms of its parametric tensor representation form (Weickert, 2001) (Wang,2004) (Tschumperlé, 2005).

PREVIOUS WORK

Spatial regularization (spatial average) reduces the corruption caused by ill-posed observation models, acquisition noise and incomplete data (Z. Li, 2001). In this sense, spatial regularization methods has been extensively used in medical image processing and in particular in Diffusion Tensor (DT) and multi DT image processing in (Tschumperlé, 2002) (Wang, 2004) (Ramirez-Manzanares, 2007) by assuming that the diffusion behaviors are similar for neighboring voxels.

We note that spatial regularization on parametric models at fiber crossing regions is challenging because we need to identify and match similar orientations between voxels with different number of fiber orientations. Secondly, often the complex structure has similar configurations only for a small set of voxels, see (Ramirez-Manzanares, 2008). Thus, a regularization framework which assumes global smoothness (Ramirez-Manzanares, 2007), may inadvertently eliminate such small anatomical structures. A better regularization approaches are based on an edge-preserving scheme (Black, 1996), which allows the regularization to break the global smoothness assumption at voxels along the boundaries between significantly different regions, thus preserving the features of each region.

In this work we propose a new anisotropic filtering scheme for the raw DW data. The filtering orientation is guided based on the knowledge we have about the axon bundle orientation. For this aim we fit DT and multi-DT models, and we use the orientation information for computing the filtering kernel. Even though reported methods for DW signal filtering exist, to the best of our knowledge there is not a reported work which uses the estimated axon bundle orientation for the computation of the anisotropic filtering.

The rest of the paper is organized as follows: In Section 2 we explain the two different models we use to estimate the local axon bundle orienta-

tion and then Section 3 presents our anisotropic filtering framework and gives implementation information. The results of our experiments on synthetic and in vivo data are presented in Section 4 and finally our conclusions are presented in Section 5.

ESTIMATION OF AXON FIBER ORIENTATION

The following subsections details two different parametric approaches to estimate the axon bundle orientation given a set of DW-MRI measurements S(qk,τ). We use such models in order to estimate the axon orientation for computing the anisotropic filtering kernels, as is explained in Section 3.

DT model fitting

In many medical applications, the angular variation of water diffusion has been extensively summarized by Diffusion Tensor (DT) model (Basser, 1996):

$$S(q_k,\tau) = S_0 \exp(-q_k^T D q_k^t) + \varepsilon_k \quad (2)$$

Where the water diffusion coefficients (with units equal to mm/s^2) are summarized by the positive definite symmetric 3×3 tensor $\mathbf{D}$. This model implicitly assumes that $P(\mathbf{x})$ presents Gaussian distribution. Given S_0 and at least six measurements $S(\mathbf{q}_k,\tau)$ in independent non–coplanar orientations, the DT can be estimated by a Least Squares procedure. The DT can be visualized as a 3D ellipsoid, with the principal axis aligned with the DT's eigenvectors and scaled by the eigenvalues λ_i. The principal eigenvector is named the Principal Diffusion Direction (PDD), and in the case of a single fiber bundle within the voxel, it is associated with the orientation of the fibers. The *fractional anisotropy* (FA) is an anisotropy measure (Basser, 1996) given by.

$$FA = \frac{\sqrt{3}}{\sqrt{2}} \frac{\sqrt{(\lambda_1-\lambda)^2+(\lambda_2-\lambda)^2+(\lambda_3-\lambda)^2}}{\sqrt{\lambda_1^2+\lambda_2^2+\lambda_3^2}} \quad (3)$$

For a DT fitted to a highly oriented diffusion within the voxel ($\lambda_1 >> \lambda_2 \simeq \lambda_3$) FA is close to one, while FA is close to zero for a DT fitted to the isotropic diffusion case ($\lambda_1 \simeq \lambda_2 \simeq \lambda_3$).

MDT model fitting

DT model assumes that water diffusion presents a single Principal Diffusion Direction at each voxel. However, at voxels where two or more fibers cross, split, or merge the DT model inadequately represents the intra–voxel diffusion (Alexander,2005). This represents a significant problem for diffusion tractography, where we rely on local orientation estimates to reconstruct fiber pathways.

A model for solving intra-voxel fiber orientations is the Gaussian Mixture Model (GMM) or multi–DT (Tuch,2002) :

$$S(q_k,\tau) = S_0 \sum_{j=1}^{L} \beta_j \exp(-q_k^T D_j q_k^T) + \varepsilon_k \quad (4)$$

Where the real–valued coefficients $\beta_j \in [0,1]$ indicate the fraction of the total diffusion associated with the tensor $\mathbf{D}_j$. Recently, in (Ramirez-Manzanares, 2007) is proposed a Diffusion Basis Functions (DBF) for GMM fitting. They simplified the fitting of model (4) by using a large tensor basis $\tilde{T}$ in the following observation model:

$$S(q_k,\tau) = \sum_{j=1}^{N} \alpha_j \varphi_{k,j} + \varepsilon_k \quad (5)$$

Where $\alpha_j \geq 0$ and the pre–computed DBF coefficients are defined as: $\varphi_{k,j} = S_0 \exp(\mathbf{q}^T_k \, \tilde{T}_j \, \mathbf{q}_k \, \tau)$. Thus, the j–*th* DBF $\{\varphi_{k,j}, k=1,\ldots,M\}$ is the DW–MRI signal due to a single fiber (modeled by the fixed basis tensor $\tilde{T}_j$) and the non-negative unknown α_j denotes its mixture contribution. This model is fitted (solved for α) by solving a linear system of equations and it is stable for recovering more than two fiber orientations per voxel. It is possible to diminish the angular error due to the discrete nature of model (5) by increasing the angular resolution of basis $\tilde{T}_j$ until it is irrelevant for practical aims.

METHODS

In this section we explain our methodology for DW signal filtering. First we introduce our idea behind the anisotropic filtering, then we present two methods for computing the filtering kernel.

Anisotropic Filtering Along Axon Fiber Orientation

The anisotropic filtering for image denoising is a well–known technique in the image processing field. For instance, in grey scale images, it is possible to compute the structure tensor based on the image's 2D gradient which principal orientation is perpendicular to object's boundaries, and then filter the image along the boundaries by using the inertia tensor (Knutsson, 1989). The prior knowledge behind this reasoning is that regions delimitated by prominent boundaries share the same features, in this case, the same grey intensity.

In case of raw DW data, we have a set of *M* different images, each one with boundaries that delimitate different regions. The prior knowledge we introduce is about the smoothness of axon bundle orientation: given that the axon bundles present a smooth trajectory, then voxels along the fiber's pathway present a similar DW signal $S(\mathbf{q}_k,\tau)$ because they share similar diffusion features. By showing two *in vivo* noisy DW signals (Figure 2) which belongs to neighboring voxels, we can how their signals are similar and also different to signal in other voxel shown in (Figure 2, left).

With this in mind it is a good idea to apply an anisotropic filtering for denoising the raw DW data. In this filtering schema a different process is applied for different voxels in the image. In this case, the local feature we use in order to select which voxels we are going to use for the filtering depends on the local orientation of the axon bundles. The *prior* information we are incorporating is well–known in DW processing: the axon bundles follow smooth trajectories along the brain, and thus it is likely to expect that neighboring voxels along the axon bundle orientation present a similar signal. Thus, if we have a local estimation of the diffusion orientation at 3D image's position *r*, then we promote a strong filtering process for signal $S_r(\mathbf{q}_k,\tau)$ with the neighboring voxels *p* along the local diffusion orientation.

In order to compute the local axon orientation we use the data provided by the single and multiple diffusion tensor models (2) and (4), respectively. Note that the multi-DT model provides not only information about the PDD, but also information about a second or third diffusion direction within voxels where the axon bundles cross, split, or merge. Moreover, the DT's shape (anisotropic information) provides a measure about the interaction between neighboring voxels: fatty tensors (with low FA) indicate prominent radial water diffusion, i.e. interaction with voxels which are perpendicular to the bundle's trajectory.

Kernel Computation for DW Filtering

Given a DT $\mathbf{D}$ at each voxel position *r*, fitted by Least Squares method from model (2), the DT's entries have the information about the local 3D orientation of the axon bundle. Given a 3D image position $r=[x,y,z]$, let N_r be the 3D second order spatial neighborhood of *r*: $N_r=\{p: |r-p|_2<2\}$ (i.e. the neighborhood is composed of 26 neighborhoods in the general case). Thus, for each voxel at *r* we compute an anisotropic kernel which indicates the expected similarity between diffusion information with respect to *p* position as:

$$w^D(r,p) = (p-r)^T D_r (p-r) \tag{6}$$

So that, if the axon bundle has an orientation similar to vector *(p−r)* then $\boldsymbol{\omega}^{\mathbf{D}}(r,p)$ has a large value, and small otherwise. On the other hand, for a multi diffusion kernel, we use the information provided by the *L* different DTs computed from DBF to fit model (4). We compute the anisotropic diffusion kernel as

$$w^{mD}(r,p) = \sum_j^L \beta_j w^{D_j}(r,p) \tag{7}$$

Where $\boldsymbol{\omega}^{D}j(r,p)$ is the diffusion kernel computed from (6) for the *j*-th DT D_j at the same position r. Given the single and multi DT diffusion kernels, we compute the denoised $\hat{S}$ signal as:

$$\hat{S}(r) = \kappa S(r) + (1-\kappa)\sum_{p\in N} \omega^D(r.p) S(p) \tag{8}$$

For the single tensor case, or using $\boldsymbol{\omega}^{\mathbf{mD}}(r,p)$ for the multi-DT case. Where $\kappa \in (0,1)$ is a scalar that weights how much we want to introduce the prior information about the neighborhood in the signal $Sr(\mathbf{q}_k,\tau)$.

Implementation details

We note in our experiments that is easier to fix the user defined parameter σ in (8) and to iterate several times the filtered signal $\hat{S}(r)$. Thus we compute iteratively $\hat{S}^t(r)$ at iteration $t=1,2,\ldots$ as follows:

$$\hat{S}^t(r) = \kappa S^{t-1}(r) + (1-\kappa)\sum_{p\in N} \omega(r.p)\hat{S}^{t-1}(p)\kappa \tag{9}$$

with $\hat{S}^0(r)=Sr(\mathbf{q}_k,\tau)$.

We apply our method only to regions of interest (ROI) inside deep white matter, to this purpose we use a threshold over the FA map and the morphological operator *erosion*, keeping all the voxels with FA value ≥ 0.35 to ensure that they are inside the white matter.

We normalize each one of $\boldsymbol{\omega}^{\mathbf{D}}(r,p)$ and $\boldsymbol{\omega}^{\mathbf{D}}{}_j(r,p)$ entries such that $\sum_{p\in N}\boldsymbol{\omega}^{\mathbf{D}}(r,p)=1$ for internal voxels as well as for voxels which lie at the boundaries of the ROI, or at the boundaries of the image, so they do not have 27 neighbors.

Experiments and Results

In order to show the performance of our method we use three different types of DW Data:

In vivo Brain Human Data. A single healthy volunteer was scanned on a Siemens Trio 3T scanner with 12 channel coil. Acquisition parameters: single-shot echo-

planar imaging, five images for b=0 s/mm^2, 64 DW images with unique, isotropically distributed orientations (b=1000 s/mm^2), TR=6 700 ms, TE=85 ms, 90^o flip angle, voxel dimensions equal to 2×2×2 mm^3. The approximated Signal to Noise Ratio (SNR) is equal to 26. For these data, we acquire 5 repetitions, so that, the ground-truth (GT) of reference S^* is computed as the average of them.

Data from a diffusion phantom. We used data acquired from a diffusion phantom (C. Poupon, 2008). Layers of hydrophobic acrylic fibres were interleaved and stack in each other to build fibre crossing configurations. Diffusion-weighted data were acquired on the 3T Tim Trio MRI systems with 12-channel. The data is available at http://www.lnao.fr/spip.php?article112. The approximated Signal to Noise Ratio (SNR) is equal to 26. For these data, we have only 2 repetitions for the GT S^* computation.

Synthetic data The DW-MRI signal was synthesized from the GMM (4). We simulate single DTs and crossings composed of two DTs. For all cases, the DT principal eigenvalue was set to 1×10^{-3} mm^2/s and the second and third tensor eigenvalues were 2.22×10^{-4} mm^2/s, FA= 0.74. The above values were taken from a sample of tensors observed in the brain data from a healthy volunteer. Rician noise was added to each measurement to produce SNR= 15. For these data, we have 5 repetitions for the S^* computation.

In all our experiments we used κ= 0.05 and the number of iterations t in (9) was equal to 8 for *in vivo* and phantom data, and 14 for synthetic data. We determine this parameter by the following empirical test: we compare the error (absolute value of the difference) between the GT and the current $\hat{S}^t$ estimation and we used the number of iterations that minimizes such an error. Figure 3 shows the result of this procedure for the *in vivo* and phantom data. Note that it is necessary to empirically determine the minimum. However this procedure must be applied only one time for each medical scan protocol, i.e. to acquire around five repetitions of *in vivo* DW data and then build a GT volume.

To assess the validity of the proposed denoising methods, for each DW acquisition the 5 other DW-MRI are averaged gradient-by-gradient, giving the GT S^*. The error between a denoised image $\hat{S}$ and the GT data is the scalar ε computed as $\varepsilon=|S^*-\hat{S}^t|$. The process is then iterated 5 times using the 5 different noisy images, yielding 5 errors, which are finally averaged to give a global error. Statistical values of these error measures are summarized on Table 1. This error computation method helps avoiding the introduction of bias.

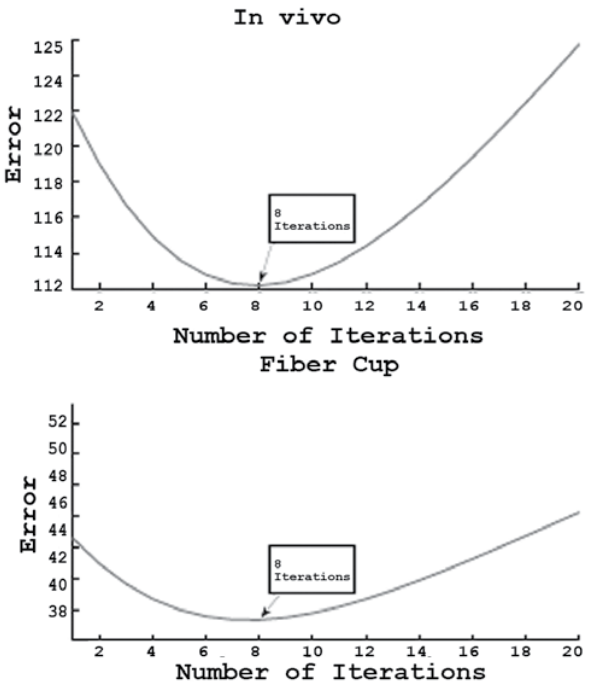

Figure 3. Evolution of error $|\hat{S} - S^*|$ along the filtering iterations. We note that 8 iterations give us the minimum error for a value γ= 0.05.

Table 1.
Statistical values for the error between the raw and filtered signals ε. Best values are in bold font.

Signal	Max ε	Min ε	*Mean ε*	StD of ε
Brain Data				
$S(\mathbf{q}_k,\tau)$	**281.0**	64.2	122.9	**23.0**
$\hat{S}$ from $\boldsymbol{\omega}^{mD}$	287.3	**56.7**	**110.0**	25.0
$\hat{S}$ from $\boldsymbol{\omega}^{D}$	287.3	*56.8*	**110.0**	25.1
Phantom Fibre Cup data				
$S(\mathbf{q}_k,\tau)$	85.7	27.9	44.6	7.0
$\hat{S}$ from $\boldsymbol{\omega}^{mD}$	**80.1**	**23.2**	**37.3**	**8.3**
$\hat{S}$ from $\boldsymbol{\omega}^{D}$	80.2	**23.2**	**37.3**	**8.3**
Synthetic data				
$S(\mathbf{q}_k,\tau)$	108.9	57.9	82.2	7.32
$\hat{S}$ from $\boldsymbol{\omega}^{mD}$	76.9	**27.2**	**40.6**	**5.8**
$\hat{S}$ from $\boldsymbol{\omega}^{D}$	**76.7**	27.5	40.7	5.9

We note that the mean and minimum values of the ε error are always smaller for the images filtered with our proposal, and in most cases for the maximum and standard deviation measures. We also note that there is not a significant difference between using single and multiple DT models for diffusion kernel computation, multi-DT presents the best values in most cases but the differences are very small. A detailed view of the distribution of the errors is presented in Figure 4, note how the error distribution for the filtered image is smaller for *in vivo* data and significantly smaller for synthetic simulations.

We present a quantitative comparison of the recovered signal $\hat{S}^t$ in Figure 5. We note that in this case (differently to the following experiments), it is hard to visually detect the improvement. However, the recovered image (in the right), like the GT, presents well defined (not blurred) brain structures.

In order to show how our methodology can improve the recovered diffusion orientations, we show the result of fitting the multi-DT model in (Gudbjartsson, 1995) for the filtered images. The cases for in vivo and synthetic data are presented in Figures 6 y 7, respectively. Qualitatively speaking, we note that the filtered images were improved in the sense that they show a better spatial orientational coherence and well aligned fiber crossings.

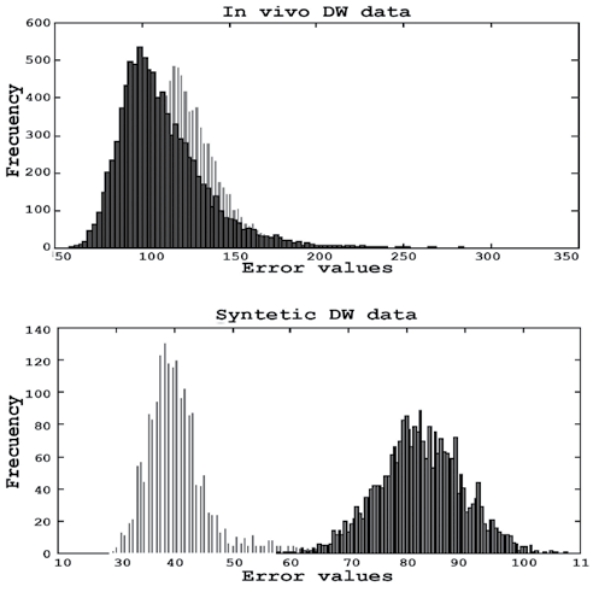

Figure 4. Noise reduction by our filtering proposal. We show the histogram of the voxel by voxel error between the raw data and the GT in red color ($|S_r(q_k, \tau) - S^*|$) and the difference of the filtered signal and the GT ($|\hat{S} - S^*|$) in blue color. Top: for in vivo DW data and; bottom: for synthetic data (the histograms for the phantom data are very similar to the *in vivo* DW data).

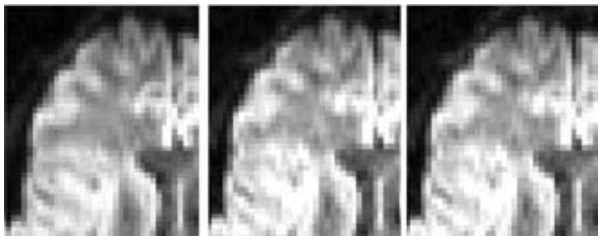

Figure 5. Qualitative comparison of DW signals on a brain axial slice. Left: Averaged S* GT, middle: raw $S(q_k, \tau)$, right: filtered $\hat{S}$.

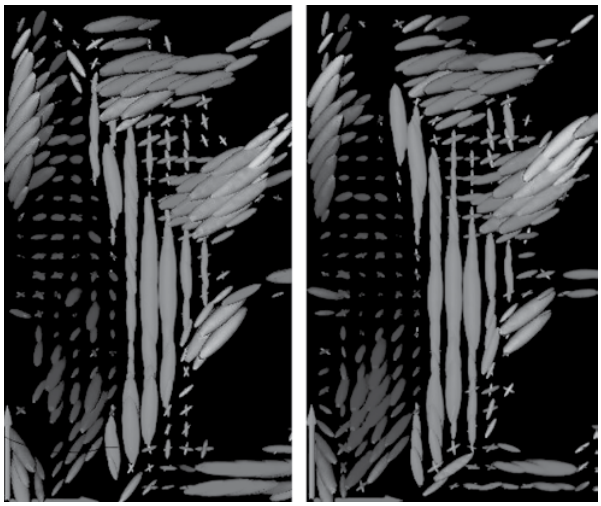

Figure 6. Filtering result on *in vivo* data. Left: DBF multi-DT fitted to raw (noisy) data. Right: DBF multi-DT fitted to filtered data. Upper- right crossing ROI (composed of green-red DTs) presents qualitative improvements.

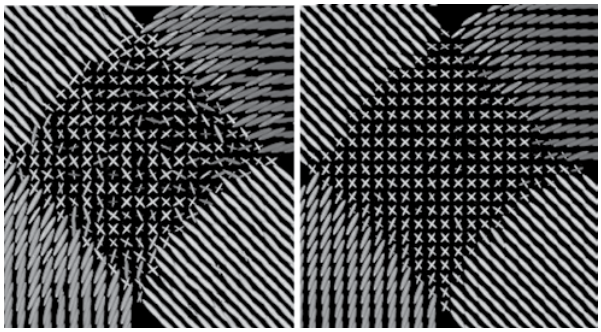

Figure 7. Synthetic fiber Crossing. Left: DBF multi-DT fitted to raw (noisy) data. Right: DBF multi-DT fitted to filtered data. Single and multi DT regions present significant improvements.

CONCLUSIONS AND DISCUSSION

We presented a new method for the anisotropic filtering of DW-MRI data. For the computation of the kernels, we used two different models: single and multi DT.

We show the advantages of the filtering by means of experiments on data from three different sources. Those experiments showed how the pernicious effect of noise is attenuated.

We compared the results for the two used models and we conclude that there is not a significant difference between the uses of them.

Finally, we depicted a methodology that can be applied to determine the best number of filtering iterations in order to obtain the best results with our proposal.

The product of this research, i.e. the Denoising of DW MRI data, is very important in two ways: a) to improve the axon pathway tractography (Basser, 2000) which follows the PDD of the tensors and b) to detect subtle axon structures, as for instance, the ones related to thin axon bundles.

As a future work we would like to test how this proposal behaves with respect to another computationally expensive parametric denoising methods that corrects single and multiple DT orientations, as for instance (Ramirez-Manzanares, 2008) (Tschumperlé,2005).

REFERENCES

Alexander D. C.(2005). An introduction to computational diffusion MRI: the diffusion tensor and beyond. *In J. Weickert and H. Hagen, editors, Visualization and Image Processing of Tensor Fields. Springer, Berlin.*

Basser P. J. and C. Pierpaoli(1996). *Microstructural and physiological features of tissues elucidated by quantitative-diffusion-tensor MRI. J. Magn. Reson.* B, 111:209–219.

Basser P. J., S Pajevic, C. Pierpaoli, J. Duda, A. Aldroubi (2000). Fiber tractography using DT-MRI data. *Magn. Reson*. Med.44:625-632.

Black M. and P. Rangarajan (1996). On the unification of line processes, outlier rejection, and robust statistics with applications in early vision. *The International Journal of Computer Vision*, 19(1):57–91.

Gudbjartsson H. and S. Patz (1995). The Rician distribution of noisy MRI data. *Magn. Reson. Med.*, 34:910–914.

Knutsson H. (1989). Representing local structure using tensors. *In Proceedings 6th Scandinavian Conf. on Image Analysis*, page 244-251, Oulu: Oulu University.

Li S. Z. (2001). Markov Random Field Modeling in Image Analysis. Springer Verlag.

Poldrack R. A. (2001) . A structural basis for developmental dyslexia: Evidence from diffusion tensor imaging. In M. *Wolf, editor, Dyslexia, Fluency, and the Brain*, pages 213–233. York Press.

Poupon C., B. R. I. Kezele, M. Perrin, F. Poupon, and J. Mangin. (2008), New diffusion phantoms dedicated to the study and validation of high-angular-resolution diffusion imaging (hardi) models. *Magn Reson Med,* 60(6):1276–1283.

Ramirez-Manzanares A., H. Zhang, M. Rivera, and J. C. Gee. (Jun. 2008) Robust regularization for the estimation of intra-voxel axon fiber orientations. *In Proc. of the workshop on MMBIA*, pages 1–8, Anchorage, Alaska.

Ramirez-Manzanares A., M. Rivera, B. C. Vemuri, P. Carney, and T. Mareci. (2007) Diffusion basis functions decomposition for estimating white matter intravoxel fiber geometry. *IEEE Trans. Med. Imag*., 26(8):1091–1102.

Tuch D. S., T. G. Reese, M. R. Wiegell, N. Makris, J. W. Belliveau, and V. J. Wedeen (2002). High angular resolution diffusion imaging reveals intravoxel white matter fiber heterogeneity. *Magn. Reson. Med.,* 48(4):577–582.

Tschumperlé D. and R. Deriche(2002) . Orthonormal vector sets regularization with PDE's and applications. *The International Journal of Computer Vision, (Special Issue VLSM),* 50:237–252.

Tschumperlé D. and R. Deriche (April 2005). Vector-valued image regularization with PDE's: A common framework for different applications. *IEEE Trans. Pattern Anal. Machine Intell.*, 27(4):506–51.

Wang Z., B. C. Vemuri, Y. Chen, and T. H. Mareci (2004). *A constrained variational principle for direct estimation and smoothing of the diffusion tensor field from complex DWI. IEEE Trans. Med. Imag.*, 23(8):930–939.

Weickert J. (2001). Diffusion and regularization methods for tensor-valued images. *In Proc. First SIAM-EMS Conf.* AMCW0.